



# A multimillennial snow water equivalent reconstruction from giant sequoia tree rings

R. Touchan<sup>1</sup> · B. Black<sup>1</sup> · E. Shamir<sup>2</sup> · M. K. Hughes<sup>1</sup> · D. M. Meko<sup>1</sup>

Received: 18 September 2020 / Accepted: 17 November 2020 / Published online: 2 January 2021  
© Springer-Verlag GmbH Germany, part of Springer Nature 2021

## Abstract

The first dendroclimatic reconstruction of May 1 snow water equivalent (SWE) was developed from a *Sequoiadendron giganteum* regional tree-ring chronology network of 23 sites in central California for the period 90–2012 CE. The reconstruction is based on a significant relationship between May 1 SWE and tree-ring growth and shows climate variability from interannual to intercentennial time scales. A regression-based reconstruction equation explains up to 55% of the variance of SWE for 1940–2012. Split-sample validation supports our use of a reconstruction model based on the full period of reliable observational data (1940–2012). Thresholds for May 1 SWE low (15 percentile) and high (80 percentile) years were selected based on the exploratory scatterplots relationship between observed and reconstructed data for the period 1940–2012. The longest period of consecutive low-SWE years in the reconstruction is 2 years and the frequency of the lowest SWE years is highest during the period 710–809 CE. The longest high-SWE period, defined by consecutive wet years, is 3 years (558–560 CE). SWE and its reconstruction positively correlate with northeastern Pacific sea surface temperatures, the low-frequency variability of which may provide some predictive ability. Ultimately, the instrumental record and reconstruction suggest that unlike other sites in the region, twentieth century SWE variability in these Sequoia groves has remained within historical boundaries and relatively buffered from extremes and severe declines, though this is likely to change in coming decades with potentially negative effects on water availability for these trees.

**Keywords** Giant sequoia · Drought · May 1 SWE · Pacific Decadal Oscillation · El Niño Southern Oscillation

## 1 Introduction

The recent drought in California has severely impacted water resources and agriculture (e.g., Howitt et al. 2014; Swain et al. 2014). The National Integrated Drought Information System (NIDIS) reported that since 2000, the longest duration of drought (D1 moderate drought–D4 exceptional drought) in California lasted 376 weeks beginning from late December 2011 to the beginning of March 2019. The most intense period of drought occurred the week of July 29, 2014, where D4 affected 58.41% of California land (<https://www.drought.gov/drought/statescalifornia>). The period of drought from 2012 to 2014 in California stands out as

among the most severe in the last 1200 years based on paleoclimate records (Griffin and Anchukaitis 2014; Seager et al. 2015; Robeson 2015; Belmecheri et al. 2016). Combined with gradually increasing air temperatures, this drought has also left dramatic regional imprints on forest health and tree mortality.

The U.S. Forest Service recently reported that 40 million trees had died across California between 2010 and late 2015, with most succumbing to drought and insect mortality from September 2014 to October 2015 alone (USFS 2016). Clark et al. (2016) indicated that prolonged drought affects distributions of species, the biodiversity of landscapes, wildfire, net primary production, and almost all goods and services provided by forests. O’Hara and Nagel (2013) reported that drought effects highlight the fundamental scale for both management and community ecology, the forest stand.

Tree-ring records from blue oak and other tree species suggest that drought conditions in the past 5 years are the most extreme in more than five centuries in southern California and the Sierra Nevada (Griffin and Anchukaitis 2014;

✉ R. Touchan  
rtouchan@ltrr.arizona.edu

<sup>1</sup> Laboratory of Tree-Ring Research, University of Arizona, Tucson, AZ, USA

<sup>2</sup> Hydrologic Research Center, San Diego, CA, USA

Belmecheri et al. 2016). What challenges do drought and climate change pose to the giant sequoia (*Sequoiadendron giganteum*)? This species, with its limited populations in 75 groves distributed over a narrow longitudinal range on the west slopes of the Sierra Nevada (Stewart et al. 1994), must withstand increasingly stressful climatic conditions. Browning canopies suggest that thresholds for survival are already being approached in some locations (<http://www.latimes.com/local/california/la-me-sequoia-drought-20150828-story.html>). Su et al. (2017) reported that the 2011–2015 drought reduced in-grove wetness by five times the 1985–2010 standard deviation. The 2011–2015 change in-grove wetness was over 50% higher than in surrounding non-grove areas, suggesting that while *Sequoiadendron giganteum* (SEGI) groves currently might serve as climate change “hydrologic” shelter within the larger mixed-conifer forest, their refugial properties may be eroding. Improved understanding of the climate sensitivity of giant sequoia tree-growth is needed for the development of strategies for mitigation and protection.

Dendrochronology is a valuable tool for the study of the relationship between climate and tree growth (Fritts 1976). It is known that extreme drought years can induce very low growth in SEGI, such that narrow rings can be used as pointers to identify years of extreme drought. Tree-ring research in the 1990s suggested that the frequency of extreme droughts in the twentieth century up to that time was close to the average for the last 2100 years (Hughes et al. 1990, 1996; Hughes and Brown 1992; Carroll et al. 2014).

There are few studies in the Sierra Nevada Mountains that have focused on the relationship between snowpack and tree-ring growth (e.g. Belmecheri et al. 2016; Lepley et al. 2020; Shamir et al. 2020). It is well known that snowpack accounts for around one-third of California’s water supply. Melting snow provides water into dry summer months characteristic of the region. Climate change became the phenomenon of the twentieth and twenty-first centuries. Understanding patterns of biological response to snowpack and snowmelt inter-annual variability is critical for managing the region’s agriculture, recreational activities, and ecology.

Lepley et al. (2020) developed a skillful, nested reconstruction for April 1 SWE, 1661–2013 CE from tree rings of montane conifer trees of the Sierra Nevada Mountains of California. The results of their study demonstrate the effectiveness of tree-rings to inform past climate variability over several centuries. Shamir et al. (2020) used a high-resolution snow-hydrologic model to derive climatological indices that describe the variability in the radial growth of four conifer species in two Sierra Nevada sites. The analysis was based on earlywood and latewood ring-width chronologies. The majority of the snowpack studies have focused on April 1 SWE in California and Colorado (Woodhouse 2003; Anderson et al. 2012; Belmecheri et al. 2016; Lepley et al. 2020;

Shamir et al. 2020). SEGI tree-ring chronologies were not included in these studies.

To the best of our knowledge, no studies have focused on using tree rings to study historic variability in the snowpack of giant sequoia (SEGI) groves. This paper describes the development of a regional tree-ring chronology of SEGI from sequoia groves, application of the chronology to develop the first dendroclimatic reconstruction of May 1 SWE specific to those groves, and linkages to broad-scale climate phenomena associated with this long-term Sequoia SWE proxy.

## 2 Methods

### 2.1 Tree-ring data

SEGI was the species used to develop the first multi-millennial tree-ring chronology (Douglass 1919, 1928). Building on the chronology developed initially by Douglass, a network of well-replicated SEGI tree-ring-width chronologies was developed by Hughes et al. (1990, 1996), Hughes and Brown (1992) and Brown et al. (1992), and four sites were updated in early and late 2011 by Meko et al. (2014, Klamath/San Joaquin/Sacramento Hydroclimatic Reconstructions from Tree Rings, Final Report to California Department of Water Resources. Accessed 15 Dec 2019, <https://cwoodhouse.faculty.arizona.edu/content/california-department-water-resources-studies>). The tree-ring data are archived at the International Tree-Ring Data Bank (ITRDB), managed by National Centers for Environmental Information NOAA and the World Data Center for Paleoclimatology. The current network covers most of the species’ geographical and ecological range (Fig. 1; Table 1). A regional chronology was developed by careful selection of a subset of tree samples without any obvious irregular growth patterns, especially surges, resembling those typically due to fire disturbance. The inter-site similarities demonstrated by visual cross-dating and computer-based quality control using the COFECHA program (Holmes 1983; Grissino-Mayer 2001) confirmed this strong common signal and justified combining all 171 series of tree-ring width measurements from the 23 sites as a single regional chronology. Each series of measured ring width was fit with a cubic smoothing spline with a frequency response of 0.50 at 67% of the series length to remove the non-climatic trends due to tree age, size, and the effects of stand dynamics (Cook and Briffa 1990). Each detrended series was prewhitened with low-order autoregressive models to remove persistence not related to climatic variations. Combining individual indices into the regional chronology was done using a bi-weight robust estimate of the mean (Cook 1985), designed to minimize the influence of outliers.

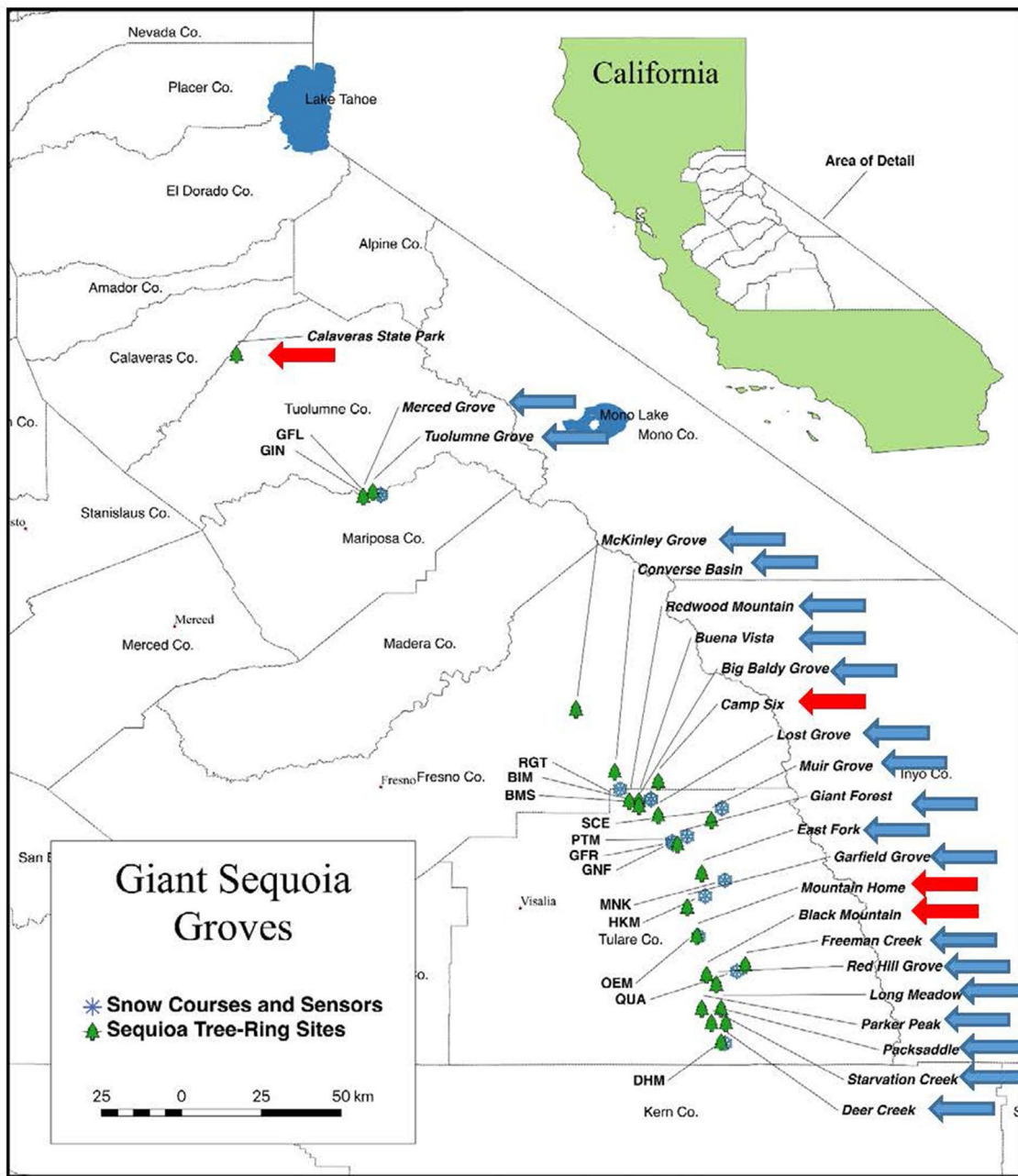


**Fig. 1** Location of the 1994 and 1996 sites collection and chronologies. The red arrows represent the four updated chronologies from Calaveras Site Park (CSP), Camp Six (CSX), Black Mountain (BMR)

and, Mountain Home (MHF) groves that were collected with other 20 SEGI chronologies in the 1990s. Time span of the four chronologies range from BC 1095-AD 2012

We used the expressed population signal (EPS) to assess the adequacy of replication in the early years of the chronology (Wigley et al. 1984). Although somewhat arbitrary, an EPS of at least 0.85 is considered adequately robust for climate reconstruction.

### 2.2 SWE data

To calculate SWE, we used the Snow-17 model (Anderson 1976) which is a mass and energy balance model that tracks the snowpack accumulation and ablation processes. The

**Table 1** Site information for giant sequoia collections in the Sierra Nevada, California

Site name	Site code	Elevation (m)	Latitude	Longitude	Time span		Total no. of years	Number of trees	No. of samples	
					(AD unless indicated)				Cores	Radials
					Earliest	Latest				
Calavers State Park	CSP	1380	38°24'	120°27'	40 BC	2011	2052	51	62	25
Tuolumne Grove	TLM	1646–1768	37°46'	119°48'	1171	1991	821	18	49	0
Merced Grove	MER	1585–1645	37°45'	119°50'	1590	1991	402	12	23	0
McKinley Grove	MKG	1890	37°01'	119°06'	1442	1992	551	21	45	0
Camp Six	CSX	2012–2164	36°46'	118°49'	351 BC	2011	2341	42	40	29
Converse Basin	CBR	1829–2073	36°48'	118°58'	1380 BC	1895	3268	41	2	39
Buena Vista	BVG	1890–2200	36°42'	118°53'	754	1991	1238	21	46	0
Redwood Mountain	RWM	5500–6700	36°42'	118°55'	105 BC	1993	2098	39	50	12
Big Baldy Grove	BBG	1951–2195	36°41'	118°53'	947	1991	1045	19	38	0
Lost Grove	LSG	2000–2040	36°39'	118°49'	1475	1991	517	13	28	0
Muir Grove	MUI	1890–2103	36°38'	118°38'	1399	1991	593	26	58	0
Giant Forest	GFO	1951–2134	36°33'	118°45'	1238 BC	1991	3230	19	15	15
East Fork	EFK	1798–2073	36°27'	118°40'	928	1991	1064	20	41	0
Garfield Grove	GAR	1707–1981	36°20'	118°43'	1275	1991	717	25	52	0
Mountain Home	MHF	2012–2042	36°14'	118°41'	1096 BC	1296	2393	18	0	24
						1297	2012	693	22	35
Freeman Creek	FCG	1830–1950	36°08'	118°31'	413	1992	1580	28	59	0
Black Mountain	BMR	1890–1981	36°06'	118°39'	211 BC	2012	2203	65	45	20
Red Hill Grove	RHG	2000–2100	36°04'	118°37'	45	1992	1948	30	57	0
Parker Peak	PPR	1737–1920	35°59'	118°40'	301 BC	1992	2293	23	36	3
Long Meadow	LMG	1952	35°59'	118°36'	326	1992	1667	32	62	0
Packsaddle	PSG	1950	35°56'	118°35'	341	1992	1652	30	60	0
Starvation Creek	SCG	1700	35°56'	118°38'	792	1992	1201	14	28	0
Deer Creek	DCG	1645	35°52'	118°36'	1324	1992	669	22	43	0

Sites are listed in order from north to south

model requires an input of sub-daily time series of precipitation and air surface temperature. We used 1918–2014 daily precipitation and temperature from the Livneh et al. (2013) gridded 6 km<sup>2</sup> climatology dataset and further disaggregated these daily time series to 6-h time steps. To represent the seasonal SWE we evaluated the daily SWE at the beginning of each winter month by averaging the simulated sub-daily SWE in the first day of each month (e.g. SWE for May 1 is the average simulated SWE of the four simulated time steps during May 1). We used the SWE simulation from Giant Forest grove (GFO; 2043 m) to represent the region. This site is located in a relatively high elevation and is in the center of the southern groves.

### 2.3 SWE reconstruction

May 1 SWE has the strongest association with the tree ring chronology. This was revealed by correlation analysis of the tree-ring index with SWE integrated over varied monthly grouping using program Seascorr (Meko et al.

2011). A transfer function analysis (TFA) was then conducted between the regional tree-ring chronology and the May 1 SWE time series. TFA is a regression model that has the regional tree-ring chronology as the predictor and selected integrated SWE time series durations as the predictand. A regression equation of SWE on the regional tree-ring chronology for the calibration period 1940–2012 was developed. Using the full period 1918–2012 was problematic in the reconstruction. The poor correlation between early-period instrumental and modeled SWE was primarily due to poor characterization of the high snowpack in the early part of the record. The validity of this equation was examined using usual regression and correlation statistics, and the predicted residual error sum of squares (PRESS) procedure was used for cross-validation (Weisberg 1985; Fritts et al. 1990; Meko 1997; Touchan et al. 2014). The PRESS method is equivalent to leave-one-out cross-validation, in which a model is validated iteratively by repeated calibration and validation, each time leaving one observation out of the calibration set and

applying the model to predict the omitted observation. Model stability was verified using a split-sample procedure (Snee 1977; Meko and Graybill 1995; Touchan et al. 2014) that divided the full period (1940–2012) into two subsets of similar length (1940–1976 and 1977–2012). The reduction of error statistic (RE), and the coefficient of efficiency (CE) (Cook et al. 1994) were calculated as a measure of reconstruction skill (Fritts 1976).

## 2.4 Identification of low and high SWE years

Individual low years and high years were defined as reconstructed May 1 SWE below or above thresholds corresponding to the specific percentiles of the simulated May 1 SWE for the years 1940–2012. The thresholds were selected from exploratory scatterplots of simulated and reconstructed SWE, taking into consideration that the threshold must be severe enough to represent a significant departure—i.e. an unusual event. The practical significance of the thresholds depends on the user of the data, which may vary among agricultural, hydrological meteorological, or socioeconomic applications. A 10-year moving average was used to summarize lower frequency changes in reconstructed May 1 SWE. A logarithmic transform ( $\log_{10}$ ) was applied to the SWE time series to correct the skewness of the data. The decision to apply this transformation was made before any analysis was performed.

## 2.5 Linkages to Pacific climate variability

The May 1 SWE index and SWE reconstructions were correlated with the monthly-averaged indices of Pacific basin-scale climate variability known to influence hydroclimate in the California region. The first of these is the Multivariate El Niño Southern Oscillation Index (MEI), defined as the leading principal component of sea level pressure, zonal and meridional components of the surface wind, sea surface temperature, surface air temperature and cloudiness in the tropical Pacific (Wolter and Timlin 1998). The other index is the “Arc” pattern, defined as the leading empirical orthogonal function of gridded North Pacific sea surface temperatures from 20° N to 180° W (Johnstone and Mantua 2014). This is an indicator of Pacific decadal variability and is similar to the Pacific Decadal Oscillation index (Mantua et al. 1997), but retains the anthropogenic warming trend and is geographically centered on the northeastern Pacific (Johnstone and Mantua 2014). Correlations were performed in the R package TreeClim with bootstrapped significance testing (Zhang and Biondi 2015).

## 3 Results

### 3.1 Chronology development

The tree-ring series of the 23 sites showed similarities in terms of visual cross-dating and computer-based quality

**Fig. 2** Giant sequoia chronologies from 23 groves for the period commencing CE 1500. Vertical axes are standardized site-level tree ring width from north (top left) to south (bottom right)

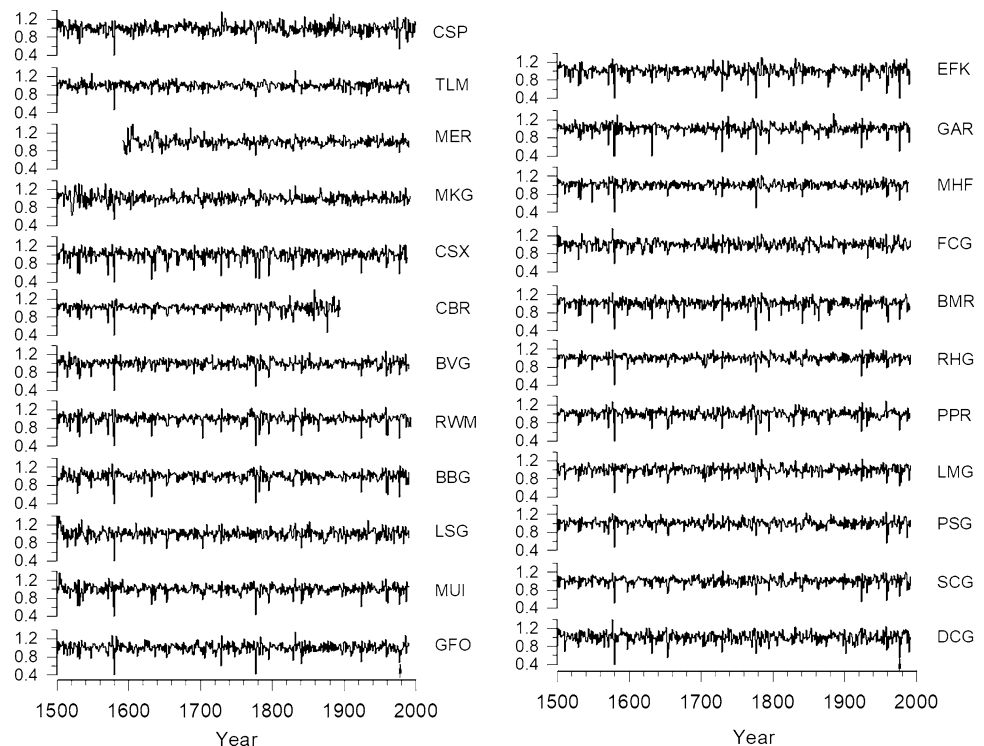


**Table 2** Correlations between giant sequoia chronologies in the Sierra Nevada, California, 1590–1895 CE (n = 306) (p < 0.001)

Site ID	CSP	TLM	MER	MKG	CSX	CBR	BVG	RWM	BBG	LSG	MUI	GFO	EFK	GAR	MHF	FCG	BMC	RHG	PPR	LMG	PSG	SCG	DCG
CSP	1.00																						
TLM	0.59	1.00																					
MER	0.39	0.46	1.00																				
MKG	0.47	0.55	0.40	1.00																			
CSX	0.41	0.54	0.37	0.59	1.00																		
CBR	0.38	0.51	0.36	0.56	0.73	1.00																	
BVG	0.31	0.45	0.36	0.56	0.73	0.64	1.00																
RWM	0.46	0.56	0.39	0.55	0.75	0.69	0.73	1.00															
BBG	0.39	0.49	0.40	0.50	0.74	0.64	0.73	0.79	1.00														
LSG	0.36	0.47	0.32	0.53	0.50	0.52	0.56	0.54	0.46	1.00													
MUI	0.41	0.53	0.40	0.55	0.75	0.70	0.74	0.82	0.74	0.61	1.00												
GFO	0.44	0.52	0.40	0.64	0.73	0.66	0.73	0.75	0.72	0.56	0.78	1.00											
EFK	0.45	0.55	0.42	0.52	0.76	0.65	0.68	0.72	0.68	0.55	0.73	0.73	1.00										
GAR	0.46	0.49	0.35	0.49	0.69	0.62	0.63	0.73	0.67	0.53	0.72	0.69	0.73	1.00									
MHF	0.48	0.50	0.41	0.56	0.65	0.62	0.66	0.72	0.65	0.55	0.74	0.75	0.73	0.72	1.00								
FCG	0.29	0.32	0.27	0.51	0.51	0.51	0.56	0.50	0.52	0.41	0.53	0.59	0.52	0.53	0.61	1.00							
BMC	0.45	0.49	0.40	0.50	0.70	0.64	0.63	0.73	0.64	0.49	0.73	0.71	0.73	0.73	0.81	0.60	1.00						
RHG	0.44	0.49	0.37	0.50	0.57	0.59	0.56	0.60	0.56	0.49	0.62	0.66	0.65	0.67	0.72	0.61	0.79	1.00					
PPR	0.41	0.48	0.36	0.51	0.70	0.65	0.60	0.72	0.67	0.49	0.70	0.74	0.72	0.73	0.77	0.60	0.82	0.75	1.00				
LMG	0.44	0.49	0.32	0.47	0.51	0.53	0.49	0.53	0.49	0.49	0.57	0.58	0.62	0.59	0.64	0.62	0.70	0.72	0.65	1.00			
PSG	0.42	0.41	0.34	0.48	0.46	0.50	0.52	0.50	0.55	0.49	0.56	0.60	0.54	0.58	0.66	0.65	0.62	0.72	0.65	0.67	1.00		
SCG	0.46	0.48	0.36	0.49	0.51	0.54	0.50	0.60	0.57	0.49	0.62	0.60	0.63	0.65	0.71	0.56	0.70	0.74	0.73	0.72	0.74	1.00	
DCG	0.47	0.46	0.37	0.45	0.53	0.53	0.45	0.54	0.52	0.46	0.55	0.56	0.61	0.63	0.63	0.47	0.63	0.68	0.70	0.61	0.64	0.74	1.00
Mean	0.43	0.49	0.37	0.52	0.61	0.58	0.58	0.63	0.60	0.49	0.64	0.64	0.63	0.62	0.65	0.513	0.647	0.613	0.644	0.565	0.558	0.597	0.556

Sites are listed in order from north to south

control. Even though the mean correlation between trees was moderate at  $r=0.27$ , the narrow rings on which most cross-dating of SEGI is based are regional in extent and strongly correspond among all site chronologies. Thus, individual trees share a high degree of common variation and are prime candidates as recorders of climate (Fig. 2; Table 2). Our results coincide with Brown et al. (1992). The combined residual chronology covers 3385 years (1372 BC–2012 AD). The mean sample segment length (MSSL) of the residual chronology is 527 years and is adequate to investigate multi-decadal climate variability (Cook et al. 1995). Given the moderate between-trees correlations, sample depth, or replication, is critical. To ensure the reliability of the reconstructed climate we restricted our analysis to the period with an EPS of at least 0.85. This threshold corresponds to a minimum sample depth of 15 trees and allows for reconstruction for the period AD 90–2012.

### 3.2 May 1 SWE reconstruction

Seascorr suggested  $\log_{10}$  May 1 SWE of the current year as the most appropriate seasonal predictand for reconstruction. The final regression statistics for the 90–2012 SWE reconstruction obtained from the relationship between the

regional tree-ring chronology (predictor) and  $\log_{10}$  May 1 SWE record (predictand) are highly significant (Fig. 3). Note that the 1-year lag of the Sequoia chronology did not significantly relate to SWE and that the standard chronology had a weaker relationship with SWE ( $R^2=0.40$ ) than the residual chronology, largely due to poor agreement in multidecadal domains (data not shown). The predictor variable accounts for 55% of simulated May 1 SWE, and the Durbin–Watson statistic had a value of 2.52, which indicates no significant autocorrelation in the regression residuals. By contrast, PRESS cross-validation regression found that SEGI accounted for only 47% of simulated April 1 SWE, an index commonly used by water managers to represent water availability from winter snowpack. The split-sample calibration–validation exercise indicated that the relationship over halves of the available instrumental data period are stable. The computed RE and CE statistics indicate skill of reconstruction in the calibration/validation exercises justifies the use of the full calibration period (1940–2012) for the final reconstruction model. The reconstruction was back-transformed from log 10 to units of mm as in the instrumental SWE record. The nearly 2000-year record is dominated by relatively high-frequency, year-to-year variability, though there are periodicities of significant power in relatively long wavelengths of 128–256 years, indicating long-term, multi-centennial fluctuations in SWE (Figs. 4, 5).

### 3.3 Identification of low and high SWE years

A scatterplot of reconstructed and observed May 1 SWE confirms the strength and linearity of the SWE signal in the tree-ring data and indicates that the reconstruction is somewhat more effective in classifying low-SWE years than in wet years (not shown). The 15th and 80th percentiles of observed SWE computed for the base period 1940–2012 correspond to natural breaks from the broader cloud of data toward outliers and were used to delineate low-SWE and high-SWE years, respectively. For the observed SWE, the 15th percentile corresponds to 545 mm or 51% of the mean; and the 80th percentile to 1502 mm or 140.402% of the mean (Fig. 4). This reconstruction was derived by linear regression of log-transformed hydrologic-model output SWE on a regional tree-ring chronology with a sample depth ranging from 15 trees in year 90 CE and 123 trees in the year 1936. Correlation of  $\log_{10}$  observed with reconstructed SWE for the 1940–2012 calibration period is  $r=0.74$ ,  $n=73$ . The correlation after back-transforming to original SWE units (mm) is  $r=0.65$ .

The long-term reconstruction for the period 90–2012 CE contains 108 low-SWE years. The maximum interval between low-SWE events is 81 years (189–270). The eighteenth century contains the highest number of low SWE years (ten events), and the longest period of consecutive

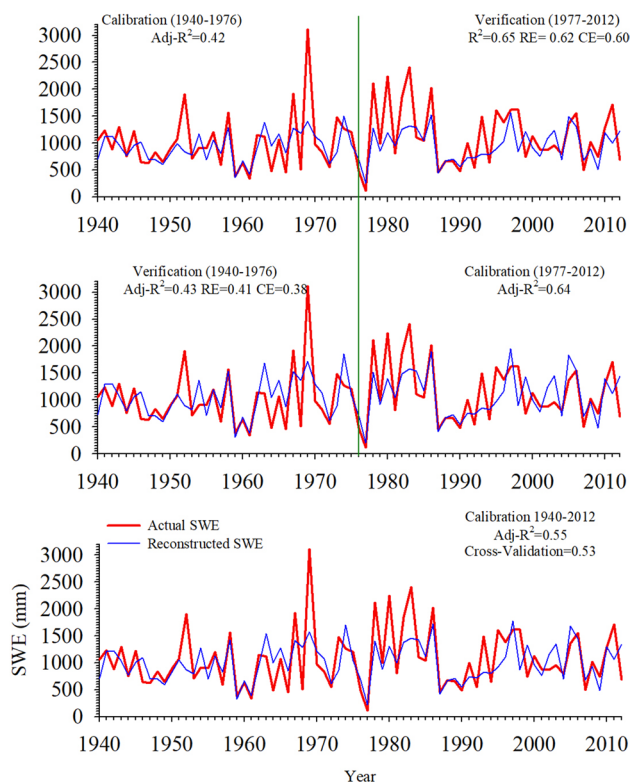


**Fig. 3** Time-series plots of actual and reconstructed May 1 SWE (mm) for the calibration and verification periods of the split sample procedure

**Fig. 4** Time series of reconstructed May 1 SWE (mm), AD 90–2012. The 80th and 15th percentiles are indicated in blue and red horizontal lines, respectively

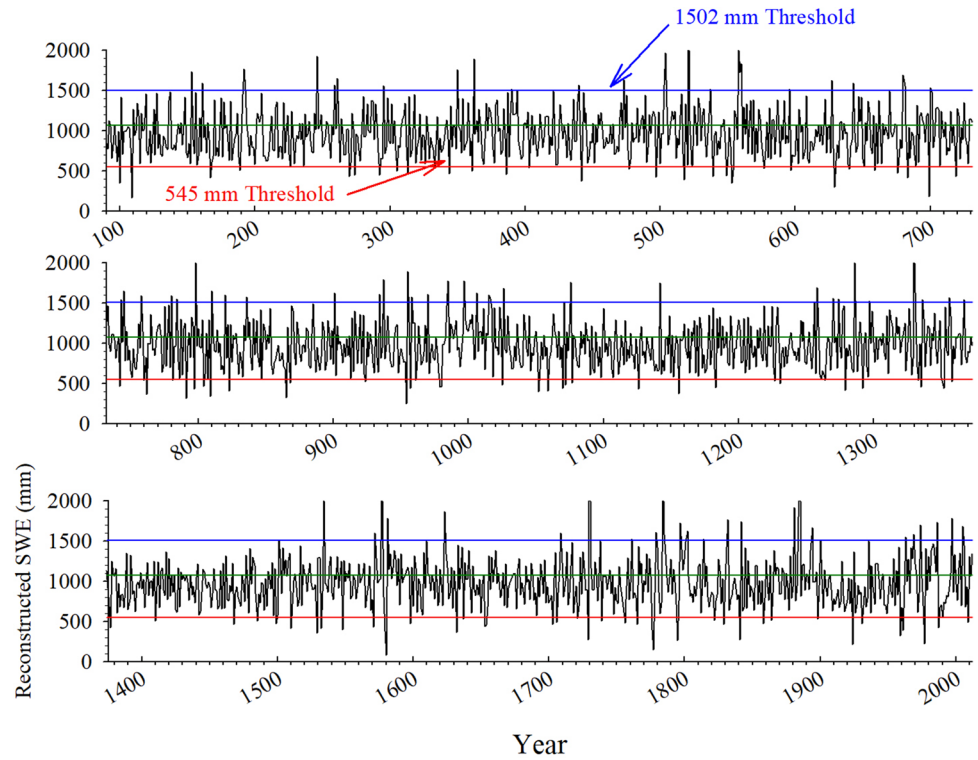
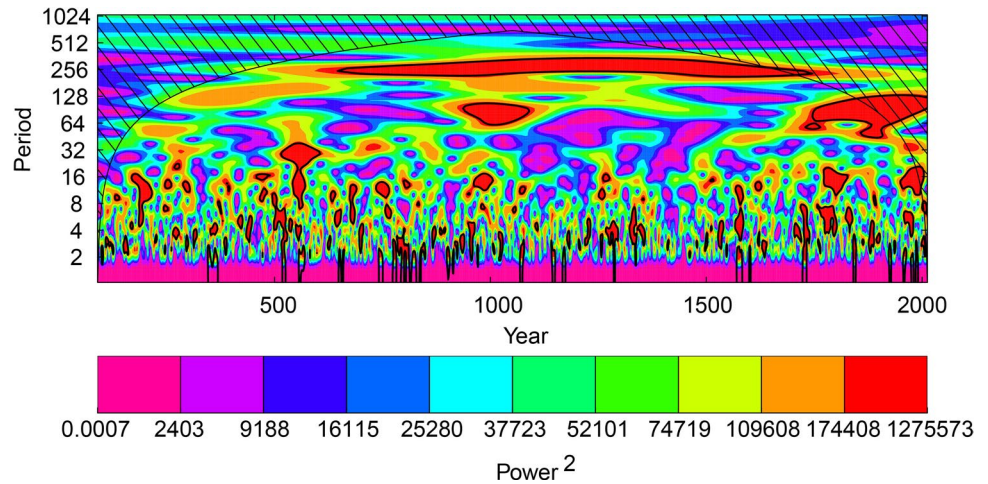


**Fig. 5** Morlet wavelet analysis of the SWE reconstruction. Regions of significance are indicated by the solid black lines and established against a red-noise spectrum at  $p < 0.1$ . Hatched lines indicate the possible edge effects of wavelengths exceeding the ends of the reconstructed time series



low-SWE years in the reconstruction is 2 years. Low-SWE events of 2 consecutive years occurred in the sixth, tenth, fourteenth, sixteenth, seventeenth, and eighteenth century, but not in the twentieth and twenty-first centuries. For the observed SWE, only one 2-year low-SWE event occurred in the twentieth century: 1976–1977. The lowest SWE year in the reconstruction was 1580 (81 mm), and the lowest in the twentieth century were 1924 and 1977 (217 mm and 220 mm respectively).

The reconstruction contains 88 high-SWE events, with a maximum interval between events of 133 years (1367–1501). The longest high-SWE period, defined by the number of

consecutive high-SWE years, is 3 years. One such event occurred in the sixth century (558–560). The highest SWE year in the reconstruction is 1730 (2569 mm). The sixth, tenth, and nineteenth century contain the most high-SWE years (eight events). The fifteenth century had no high-SWE events.

### 4 Discussion

Carroll et al. (2014) reported that there was no significant relationship between SEGI tree-ring width chronologies, snowpack, snowmelt, and associated soil moisture. In



contrast we show that SEGI can explain more than half the variance of May 1 SWE in the model calibration period and provide almost 2000 years of accurate SWE reconstruction. However, we note that in our study we have screened the available SEGI tree-ring data to eliminate trees whose ring-width patterns are clearly distorted by fire, and that we are using a SWE simulations that more directly reflects available moisture at the end of the winter season.

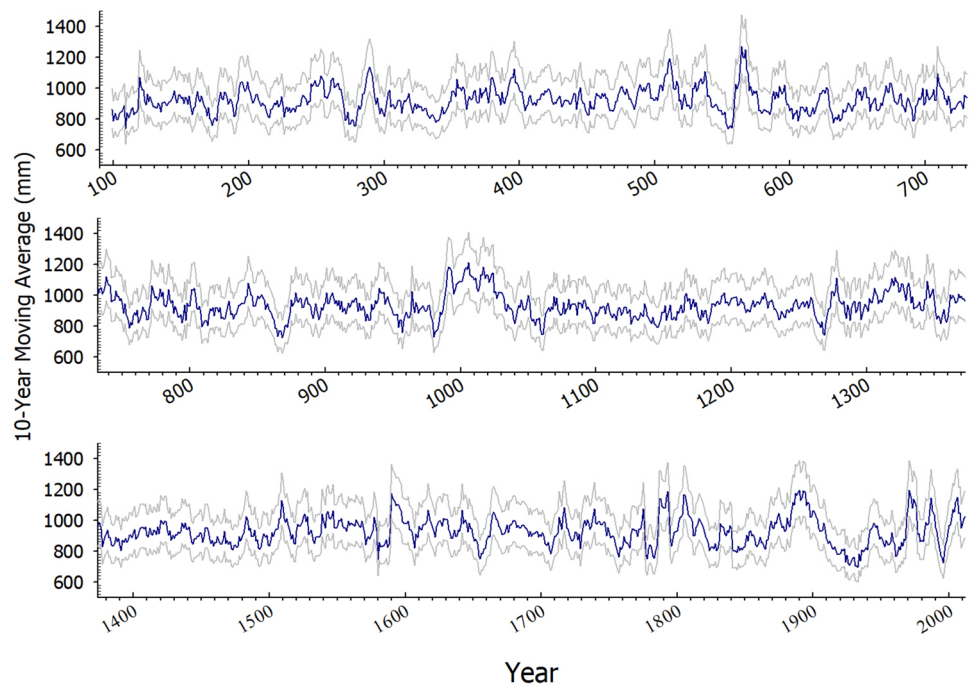
Temperature plays an important role on SWE variability. Cayan (1996) found that California winter/spring temperatures were cooler for years with high SWE and warmer for years with low SWE with the greatest differences occurring after April 1, consistent with our finding that a reconstruction of May 1 SWE is more robust than of April 1 SWE. Westerling et al. (2006) showed that increasing frequencies of large fires (> 1000 acres) across the western United States since the 1980s were strongly linked to increasing temperatures and earlier spring snowmelt. Stephenson (1988) reported that greater spring snow depth and more persistent snow might yield greater water availability during the spring and summer growing seasons at lower altitudes where snowmelt occurs about 1 month earlier than at treeline. Su et al. (2017) indicated that SEGI groves wetness is extremely sensitive to drought. The impact of droughts on the wetness of SEGI groves reflected influences of both the multi-decadal increase in forest biomass and the effects of warmer drought-year temperatures on the evaporative demand of current grove vegetation, versus available “regolith” water storage of rain and snowmelt vegetation through dry periods.

It should be emphasized that the reconstruction likely underestimates the true frequency of low and high SWE

periods when these events are defined by a specified level of observed SWE, as done here. This bias arises from the compression of regression estimates towards the calibration-period mean, as evident in the time-series plots of observed and reconstructed SWE (Fig. 2). For example, this treatment of the reconstruction fails to identify the 1976–1977 SWE event of 2 years in the observed SWE in the twentieth century. Reconstructed SWE was low in 1976, but failed to reach the low-SWE threshold. We also note that the years prior to 1976 had unusually high SWE. Possibly some carryover in food storage or other biological factors from those years kept 1976 from dropping as much as if SWE were normal in the preceding years. Our use of residual chronologies should reduce but perhaps may not eliminate the effects of tree-ring persistence in distorting the reconstruction. A 10-year moving average of the SWE reconstruction demonstrates multiannual to decadal variation and suggests several prolonged low and high SWE events (Fig. 6). The lowest SWE 10-year reconstructed period was 1923–1932 (699 mm). The highest SWE 10-year reconstructed period was 556–565 (1236 mm).

The sum of low reconstructed years of May 1 SWE in a 100-year sliding window, restricted to the more robust 90–2012 CE part of the reconstruction, shows that the frequency of lowest SWE years is highest during the period 710–809 CE (Fig. 7). Results here can be compared with information on century-scale droughts gleaned from exposed stumps in rivers and lakes in the Sierra Nevada and surrounding areas, which suggest drought lasting more than 200 years ending ~ 1112 CE, and drought lasting more than 140 years ending ~ 1350 CE (Stine 1994). The Sequoia does

**Fig. 6** Ten-year moving average of reconstructed May 1 SWE. Values are plotted at the last year of each 10 year period for the 90–2012 reconstruction. Grey line represent uncertainty values at 80% confidence interval.



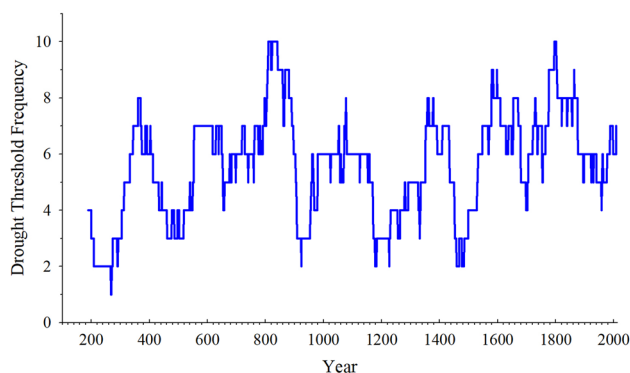


**Fig. 7** Time plot of sum of dry years in a moving 100-year window. Sum plotted at the end of 100-year period

show a peak in frequency of low-SWE years for 100-year periods ending in the early 1100s; a major peak in frequency also occurs in the 1350s, but somewhat later than 1350. Stine (1994) drought peaks are supported by tree-ring data in the context of hydrologic modeling (Graham and Hughes 2007). It should be recognized that epochs of droughts leading to drying up of lakes, as reflected by stumps (e.g., Stine 1994) may not exactly correspond to droughts summarized by a frequency of low-SWE years because the former can result from a long period of a lack of normal and high-runoff years, and not necessarily require intense drought in individual years.

Although correlations are low, this Sequoia-based SWE reconstruction significantly relates with the Belmecheri et al. (2016) ( $R^2=0.18$ ;  $p<0.001$ ; 481 years common interval) reconstruction of Southern Sierra Nevada SWE and Lepley et al. (2020) ( $R^2=0.13$ ;  $p<0.001$ ; 398 years common interval) SWE reconstruction for the American River in the Central Sierra Nevada. The relationship, especially with the Belmecheri et al. (2016), is heteroscedastic such that there is more agreement in negative, low SWE years. Yet unlike other SWE reconstructions in the California Sierra Nevada (Belmecheri et al. 2016; Lepley et al. 2020) and even in the northern Cascade Mountains (Harley et al. 2020), 2015 in the Sequoia groves is not the lowest snowpack year in the reconstruction or even in the instrumental record. From 1940 to 2015, the interval of the simulated record for which there is more confidence, the lowest snowpack years are 1977 followed by 2015. There may have been at least six additional years of snowpack lower than 2015 in the early portion of the record between 1915 and 1939, though there is uncertainty as to the accuracy of these data. There is also no apparent decline in snowpack over the past century. Thus, the regional topography and climate may be buffering Sequoia groves and delaying the inevitable snowpack declines that will occur under increasingly warmer temperatures. If Sequoia trees are already showing signs of stress, future changes may

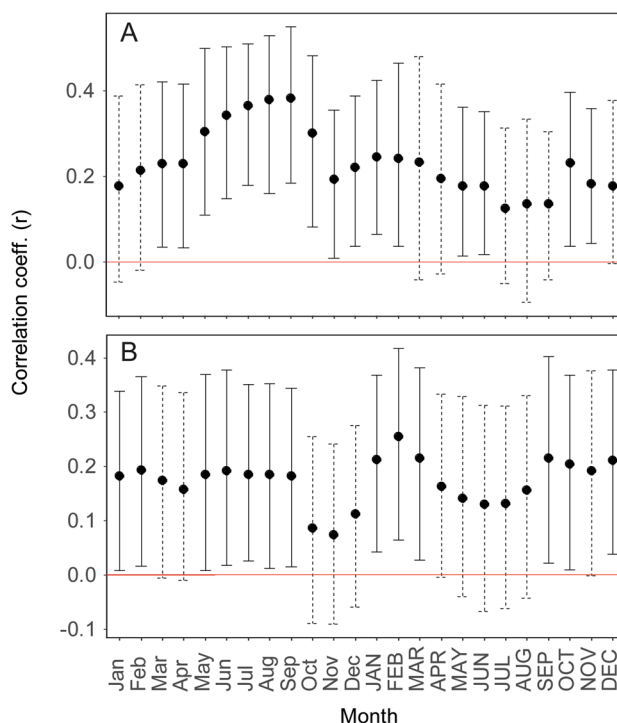


**Fig. 8** Correlation with bootstrapped confidence intervals ( $p<0.05$ ) between monthly-averaged “Arc” index and **a** simulated May 1 SWE and **b** reconstructed SWE from Sequoia

be deleterious, and monitoring will be critical for capturing when those inflection points are reached.

Interannual variability in the snowpack is linked to broad-scale climate patterns in the Pacific Ocean. Although SWE did not significantly correlate to monthly MEI of the current or prior year, the May 1 SWE simulation significantly correlated ( $p<0.05$ ) to the Arc pattern from the prior March through the current February, peaking in the prior warm-season months of July–September (Fig. 8). The reconstruction followed a similar seasonality, but with weaker correlations peaking in the prior Jul–Sep and current Jan–Mar (Fig. 8). The El Niño Southern Oscillation (ENSO) strongly influences cool-season precipitation in California, driven in large part via teleconnections with the winter North Pacific High, the strength of which blocks or facilitates the Pacific storm track and thus the delivery of moisture to the southwestern US (Schwing et al. 2002; Hartmann 2015; Seager et al. 2015; Black et al. 2018). Tree-ring chronologies in this region, especially at a lower elevation, are sensitive to this teleconnected pattern (Stahle et al. 2013; Wilson et al. 2010). However, the relationship between ENSO and precipitation is weak in the Sierra Nevada (Schonher and Nicholson 1989). Consistent with this geographic pattern simulated SWE as well as SWE reconstructed from Sequoia do not appear to capture ENSO signals. Beyond ENSO, there

is a strong precedent of a significantly positive relationship between Pacific decadal variability and snowpack in the Sierra Nevada Mountains (Mote 2006), which is also widely reflected in tree-ring chronologies from this region (St George 2014). Indeed, there is significant power in the 16–32 years wavelengths consistent with the periodicity of Pacific decadal variability (Fig. 5). Thus, the multidecadal stanzas of regime shifts in the North Pacific may provide at least some predictive value for snowpack in these Sequoia groves.

## 5 Conclusion

This paper presents the first May 1 SWE reconstruction (92–2012 CE) developed using SEGI tree-ring data. Our reconstruction provides vital information concerning low and high SWE variability in central California. Extending annual observed climatic data through dendrochronology offers new perspectives on the level, variability, and duration of past climatic trends and extreme events.

Multi-year to decadal variations in May 1 SWE are evident from our reconstruction. According to our reconstruction, the longest period of low-SWE is 2 years. Two low-SWE events of 2 consecutive years occurred in the sixth, tenth, fourteenth, sixteenth, seventeenth, and eighteenth centuries, but not in the twentieth and twenty-first centuries. For the observed SWE, only one 2-year low-SWE event occurred in the twentieth century: 1976–1977. The lowest SWE year in the reconstruction was 1580 (81 mm), and the lowest in the twentieth century was 1924 and 1977 (217 mm and 220 mm respectively). Variability in the reconstruction has no clear relationship to the El Niño Southern Oscillation but does correlate with interdecadal variability in the northeastern Pacific. Finally, the presented methodology enriched interpretations of the hydroclimatic history of recent centuries and millennia as recorded by SEGI tree rings. Updating the 23 SEGI chronologies would add at least 28 years and help to understand the response of tree growth to recent climate extremes including major El Niño events, droughts, and trends in rising hydroclimatic variability.

**Acknowledgements** We want to thank the extensive group that contributed to chronology development that were mentioned in Brown et al. (1992), Hughes and Brown (1992), and Hughes et al. (1996). We also want to thank Edward W. Wright, Martin Munro, Mark Losleben, Alma Piermattei, and Ellis Margolis, and Kai Lepley for their contribution. Funding was provided by Cooperative Agreement CA 8018-1-002, CA8033-1-0002, CA 8032-1-0002 with the USDI National Park Service, WaterSmart Program-Bureau of Reclamation Agreement # R11 AP 81 457, NSF Grant Earth Science–Hydrologic Sciences (Award No. 1445895 and 1445889), and Save the Redwoods League.

## References

- Anderson EA (1976) A point energy and mass balance model of a snow cover, NOAA Tech. Rep. NWS 19. National Oceanic and Atmospheric Administration, Silver Spring, Md, pp 150
- Anderson S, Moser CL, Tootle GA, Grissino-Mayer HD, Timilsena J, Piechote T (2012) Snowpack reconstructions incorporating climate in the Upper Green River Basin (Wyoming). *Tree Ring Res* 68(2):105–114. <https://doi.org/10.3959/2011-8.1>
- Belmecheri S, Babst F, Wahl ER, Stahle DW, Trouet V (2016) Multi-century evaluation of Sierra Nevada snowpack. *Nat Clim Change* 6(1):2. <https://doi.org/10.1038/nclimate2809>
- Black BA, Van der Sleen P, Di Lorenzo E, Sydeman WJ, Griffin D, Garcia-Reyes M, Rykaczewski RR, Bograd SJ, Dunham JB, Safeeq M, Arismendi I (2018) Rising synchrony controls western North American ecosystems. *Glob Change Biol* 24:2305–2314. <https://doi.org/10.1111/gcb.14128>
- Brown PM, Hughes MK, Baisan CH, Swetnam TW, Caprio AC (1992) Giant sequoia ring-width chronologies from the central Sierra Nevada, California. *Tree Ring Bull* 52:1–14
- Carroll AL, Sillett SC, Kramer RD (2014) Millennium-scale crossdating and inter-annual climate sensitivities of standing California redwoods. *PLoS ONE* 9(7):e102545
- Cayan DR (1996) Interannual climate variability and snowpack in the western United States. *J Clim* 9:928–948
- Clark JS, Iverson L, Woodall CW, Allen CD et al (2016) The impacts of increasing drought on forest dynamics, structure, and biodiversity in the United States. *Glob Change Biol* 2016(22):2329–2352. <https://doi.org/10.1111/gcb.13160>
- Cook ER (1985) A time series analysis approach to tree-ring standardization. Unpublished PhD. dissertation, University of Arizona, Tucson
- Cook ER, Briffa K (1990) A comparison of some tree-ring standardization methods. In: Cook ER, Kairiukstis LA (eds) *Methods of dendrochronology: applications in the environmental sciences*. Springer, New York, pp 153–162
- Cook ER, Briffa KR, Jones PD (1994) Spatial regression methods in dendroclimatology: a review and comparison of two techniques. *Int J Climatol* 14:379–402
- Cook ER, Briffa KR, Meko DM, Graybill DS, Funkhouser G (1995) The ‘segment length curse’ in long tree-ring chronology development for paleoclimatic studies. *Holocene* 5(2):229–237
- Douglass AE (1919) Climatic cycles and tree-growth: a study of the annual rings of trees in relation to climate and solar activity. In: Carnegie Inst Washington, vol 289
- Douglass AE (1928) Climatic cycles and tree growth: vol. II. In: Carnegie Inst Washington, vol 289
- Fritts H (1976) *Tree rings and climate*. Academic Press, London
- Fritts HC, Guiot J, Gordon GA et al (1990) Methods of calibration, verification and reconstruction. In: Cook ER and Kairiukstis LA (eds) *Methods of dendrochronology: applications in the environmental sciences (International Institute for Applied Systems Analysis)*. Boston, MA: Kluwer Academic Publishers, pp 163–176
- Graham NE, Hughes MK (2007) Reconstructing the mediaeval low stands of Mono Lake, Sierra Nevada, California, USA. *Holocene* 17(8):1197–12102
- Griffin D, Anchukaitis KJ (2014) How unusual is the 2012–2014 California drought? *Geophys Res Lett* 41(24):9017–9023
- Grissino-Mayer HD (2001) Evaluating crossdating accuracy: a manual and tutorial for the computer program COFECHA. *Tree Ring Res* 57:205–221
- Harley GL, Maxwell RS, Black BA, Bekker MF (2020) A multi-century, tree-ring-derived perspective of the North Cascades (USA) 2014–2016 snow drought. *Clim Change*. <https://doi.org/10.1007/s10584-020-02719-0>

- Hartmann DL (2015) Pacific sea surface temperature and the winter of 2014. *Geophys Res Lett* 42:1894–1902
- Holmes RL (1983) Computer-assisted quality control in tree-ring dating and measurement. *Tree Ring Bull* 43:68–78
- Howitt R, Medellín-Azuara J, MacEwan D, Lund J, Sumner DA (2014) Economic analysis of the 2014 drought for California agriculture center for watershed sciences. University of California, Davis, p 16
- Hughes MK, Brown PM (1992) Drought frequency in central California since 101 BC recorded in giant sequoia tree rings. *Clim Dyn* 6(3–4):161–167
- Hughes MK, Richards BJ, Swetnam TW, Baisan CH (1990) Can a climate record be extracted from giant sequoia tree rings? In: Betancourt JL, Tharp VL (eds) Proceedings of the sixth annual Pacific climate (PACCLIM) workshop. Technical report, 23. Interagency ecological studies program for the sacramento-san joaquin estuary, California Department of Water Resources, pp 111–114
- Hughes MK, Touchan R, Brown PM (1996) A multimillennial network of giant sequoia chronologies for dendroclimatology. In: Meko DM (ed) Tree rings, environment and humanity. Tucson, AZ: Radiocarbon, pp 225–234
- Johnstone JA, Mantua NJ (2014) Atmospheric controls on northeast Pacific temperature variability and change, 1900–2012. *Proc Natl Acad Sci USA* 111:14360–14365
- Lepley K, Touchan R, Meko DM, Shamir E, Graham R, Falk D (2020) snowpack reconstruction modeled using upper-elevation coniferous. Holocene. <https://doi.org/10.1177/0959683620919972>
- Livneh B, Rosenberg EA, Lin C, Nijssen B, Mishra V, Andreadis KM et al (2013) A long-term hydrologically based dataset of land surface fluxes and states for the conterminous United States: update and extensions. *J Clim* 26:9384–9392. <https://doi.org/10.1175/jcli-d-12-00508.1>
- Mantua NJ, Hare SR, Zhang Y, Wallace JM, Francis RC (1997) A Pacific interdecadal climate oscillation with impacts on salmon production. *Bull Am Meteorol Soc* 78:1069–1079
- Meko DM (1997) Dendroclimatic reconstruction with time varying subsets of tree indices. *J Clim* 10:687–696
- Meko DM, Graybill DA (1995) Tree-ring reconstruction of Upper Gila River discharge. *J Am Water Resour Assoc* 31:605–616
- Meko DM, Touchan R, Anchukaitis KJ (2011) Seascorr: a MATLAB program for identifying the seasonal climate signal in an annual tree-ring time series. *Comput Geosci* 37:1234–1241
- Meko DM, Woodhouse CA, Touchan R (2014) Klamath/San Joaquin/Sacramento hydroclimatic reconstructions from tree rings. Final Report to California Department of Water Resources. Agreement 4600008850. <https://cwoodhouse.faculty.arizona.edu/content/california-department-water-resources-studies>. Accessed 15 Dec 2019
- Mote PW (2006) Climate-driven variability and trends in mountain snowpack in western North America. *J Clim* 19:6209–6220
- O'Hara KL, Nagel LM (2013) The stand: revisiting a central concept in forestry. *J For* 111:335–340
- Robeson SM (2015) Revisiting the recent California drought as an extreme value. *Geophys Res Lett* 42(16):6771–6779
- Schonher T, Nicholson S (1989) The relationship between California rainfall and ENSO events. *J Clim* 2:1258–1269. [https://doi.org/10.1175/1520-0442\(1989\)002%3c1258:TRBCRA%3e2.0.CO;2](https://doi.org/10.1175/1520-0442(1989)002%3c1258:TRBCRA%3e2.0.CO;2)
- Schwing FB, Murphree T, deWitt L, Green PM (2002) The evolution of oceanic and atmospheric anomalies in the northeast Pacific during the El Niño and La Niña events of 1995–2001. *Prog Oceanogr* 54:459–491. [https://doi.org/10.1016/S0079-6611\(02\)00064-2](https://doi.org/10.1016/S0079-6611(02)00064-2)
- Seager R, Hoerling M, Schubert S, Wang HL, Lyon B, Kumar A, Nakamura J, Henderson N (2015) Causes of the 2011–14 California drought. *J Clim* 28:6997–7024
- Shamir E, Meko DM, Touchan R, Lepley KS, Campbell R, Kaliff RN, Georgakakos KP (2020) Snowpack- and soil water content-related hydrologic indices and their association with radial growth of conifers in the Sierra Nevada, California. *J Geophys Res Biogeosci* 125:e2019JG005331. <https://doi.org/10.1029/2019JG005331>
- Snee RD (1977) Validation of regression models: methods and examples. *Technometrics* 19:415–428
- St. George S (2014) An overview of tree-ring width records across the Northern Hemisphere. *Quat Sci Rev* 95:132–150
- Stahle DW, Griffin RD, Meko DM, Therrell MD, Edmondson JR, Cleaveland MK, Stahle LN, Burnette DJ, Abatzoglou JT, Redmond KT, Dettinger MD, Cayan DR (2013) The ancient blue oak woodlands of California: longevity and hydroclimatic history. *Earth Interact* 17:1–23. <https://doi.org/10.1175/2013ei000518.1>
- Stephenson NL (1988) Climatic control of vegetation distribution: the role of the water balance with examples from North America and Sequoia National Park. California. Ph.D. dissertation. Cornell University, Ithaca, NY, p 295
- Stewart DM, Key SH, Waldron BA, Rogers RR (1994) Giant sequoia management in the national forests of California, PSW GTR-91 USDA For. Serv., Visalia, CA, pp 152–158
- Stine S (1994) Extreme and persistent drought in California and Patagonia during medieval time. *Nature* 369:546–549
- Su Y, Bales RC, Ma Q, Nydick K, Ray RL, Li W, Guo Q (2017) Emerging stress and relative resiliency of Giant Sequoia groves experiencing multi-year dry periods in a warming climate. *J Geophys Res Biogeosci*. <https://doi.org/10.1002/2017JG004005>
- Swain DL, Tsiang M, Haugen M, Singh D, Charland A, Rajaratnam B, Diffenbaugh NS (2014) The extraordinary California drought of 2013/2014: character, context, and the role of climate change. *Bull Am Meteorol Soc* 95(9):S3–S7
- Touchan R, Christou AK, Meko DM (2014) Six centuries of May–July precipitation in Cyprus from tree rings. *Clim Dyn* 43:3281–3292
- USFS (2016) <https://www.fs.usda.gov/news/releases/forest-service-survey-finds-record-66-million-dead-trees-southern-sierra-nevada>. Accessed 22 June 2016
- Weisberg R (1985) Applied linear regression. Wiley, New York
- Westerling AL, Hidalgo HG, Cayan DR, Swetnam TW (2006) Warming and earlier spring increase western U.S. forest wildfire activity. *Science* 313(5789):940–943. <https://doi.org/10.1126/science.1128834>
- Wigley T, Briffa K, Jones P (1984) On the average value of correlated time series, with applications in dendroclimatology and hydrometeorology. *J Appl Meteorol Climatol* 23:201–213
- Wilson R, Cook E, D'Arrigo R, Riedwyl N, Evans MN, Tudhope A, Allan R (2010) Reconstructing ENSO: the influence of method, proxy data, climate forcing and teleconnections. *J Quat Sci* 25(1):62–78
- Wolter K, Timlin MS (1998) Measuring the strength of ENSO events - how does 1997/98 rank? *Weather* 53:315–324
- Woodhouse CA (2003) A 431-yr reconstruction of western Colorado snowpack from tree rings. *J Clim* 16(10):1551–1561
- Zhang C, Biondi F (2015) Treeclim: an R package for the numerical calibration of proxy-climate relationships. *Ecography* 38:431–436. <https://doi.org/10.1111/ecog.01335>

**Publisher's Note** Springer Nature remains neutral with regard to jurisdictional claims in published maps and institutional affiliations.